Chemosphere 340 (2023) 139806

Contents lists available at ScienceDirect

Chemosphere

journal homepage: www.elsevier.com/locate/chemosphere

Comparing the adsorption of methyl orange and malachite green on similar yet distinct polyamide microplastics: Uncovering hydrogen bond interactions

Kangkang Wang [a,b], Yuli Kou [a], Kefu Wang [a], Siqi Liang [a], Changyan Guo [a], Wei Wang [b,*], Yi Lu [a,**], Jide Wang [a,***]

[a] Xinjiang Key Laboratory of Oil and Gas Fine Chemicals, School of Chemical Engineering and Technology, Xinjiang University, Urumqi, 830046, China
[b] Department of Chemistry and Centre for Pharmacy, University of Bergen, Bergen, 5007, Norway

HIGHLIGHTS

- Evaluated methyl orange (MO) and malachite green (MG) sorption on microplastics.
- Competitive adsorption of MO and MG observed on Polyamide (PA).
- PH influences coexisting MO and MG adsorption.
- Stronger MO and MG adsorption on PA6 than PA66 due to hydrogen bonding.
- Simulated body fluid facilitates easier MO and MG desorption compared to fresh water.

GRAPHICAL ABSTRACT

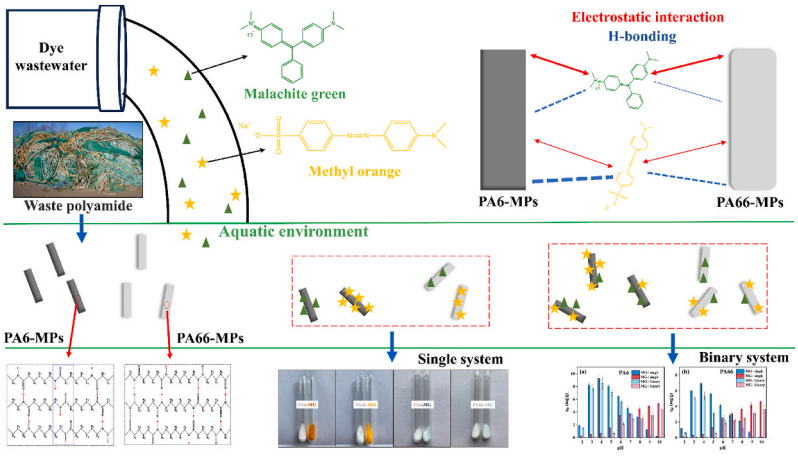

ARTICLE INFO

Handling editor: Yongmei Li

Keywords:
Polyamide microplastics
Methyl orange
Malachite green
Adsorption mechanism

ABSTRACT

Microplastics (MPs) and dye pollutants are widespread in aquatic environments. Here, the adsorption characteristics of anionic dye methyl orange (MO) and cationic dye malachite green (MG) on polyamide 6 (PA6) and polyamide 66 (PA66) MPs were investigated, including kinetics, isotherm equilibrium and thermodynamics. The co-adsorption of MO and MG under different pH was also evaluated. The results reveal that the adsorption process of MO and MG is suitably expounded by a pseudo-second-order kinetic model. The process can be characterized by two stages: internal diffusion and external diffusion. The isothermal adsorption equilibrium of MO and MG can be effectively described using the Langmuir model, signifying monolayer adsorption. Furthermore, the thermodynamic results indicated that the adsorption was spontaneous with exothermic and

* Corresponding author.
** Corresponding author.
*** Corresponding author.
E-mail addresses: wei.wang@uib.no (W. Wang), luyi_xjzjy@163.com (Y. Lu), awangjd@sina.cn (J. Wang).

https://doi.org/10.1016/j.chemosphere.2023.139806
Received 5 May 2023; Received in revised form 7 August 2023; Accepted 11 August 2023
Available online 11 August 2023

endothermic properties, respectively. The results of binary systems reveal that MO dominates the adsorption at low pH (2–5), while MG dominates at high pH (8–10). Strong competitive adsorption was observed between MO and MG in neutral conditions (pH 6–8). The desorption experiments confirm that PA6 and PA66 could serve as potential carriers of MO and MG. The interaction between dyes and polyamide MPs is primarily mediated through hydrogen bonds and electrostatic attraction. The results reveal that PA6 formed more hydrogen bonds with the dyes, resulting in higher adsorption capacity than that of PA66. This difference can be attributed to the disparities in the synthesis process and polymerization method. Our study uncovered the adsorption mechanism of dye pollutants on PA6 and PA66, and provided a more comprehensive theoretical basis for the risk assessment concerning different types of polyamide MPs in aquatic environments.

1. Introduction

Plastic products are widely produced and used worldwide due to their quality and affordability. However, an alarming 320 million tons of plastic waste is recklessly discharged into the environment every year, causing a serious environmental burden (Wu et al., 2019). These discarded plastics undergo physical, chemical and biological processes and eventually break down into minuscule plastic particles (Liu et al., 2023). These plastic particles, with size of 5 mm or less, are commonly known as microplastics (MPs) (Wang et al., 2023a). As a new type of pollutant, MPs persist in aquatic environment. Aquatic organisms ingest MPs, which adversely affects their growth, behavior, and development (Missawi et al., 2022; Wang et al., 2023b). Furthermore, MPs exhibit a robust hydrophobicity and large surface area, making them highly efficient at adsorbing pollutants such as phenanthrene (Zhao et al., 2020), naphthalene (Yu et al., 2020a), and tetracycline (Wang et al., 2021a). Na et al. reported that diphenylketone-3 and polyethylene (PE) MPs manifest a synergistic effect, amplifying the toxic effect on large water fleas (Na et al., 2021). This confirms the insidious potential of MPs to accumulate and propagate through the food chain, thereby jeopardizing aquatic ecosystems and food security (Lee et al., 2019; Barboza et al., 2020). Understanding the adsorption mechanism between MPs and pollutants and exploring the desorption behavior of contaminated MPs in body fluids is essential to ensure the protection of the ecological environment and risk assessment.

The mechanisms of adsorption between various types of MPs and pollutants vary (Lončarski et al., 2021). In the study conducted by Yu et al. the adsorption mechanism of benzotriazole and benzothiazole on polyvinyl chloride (PVC) MPs was investigated, affirming that electrostatic and hydrophobic interactions predominantly govern the adsorption of pollutants on PVC (Yu et al., 2022). Surface adsorption was confirmed to be the primary adsorption mechanism for imidacloprid, thiamethoxam, and benomyl on PE by Li et al. (2021a). Using DFT calculations, Mo et al. assisted in determining the adsorption mechanisms of chlorpyrifos and carbendazim on polypropylene (PP) MPs and PE MPs, and the findings confirmed that intermolecular van der Waals forces are the primary adsorption mechanism (Mo et al., 2021). The adsorption of Cu(II) by polystyrene (PS) MPs and polyethylene terephthalate (PET) MPs in simulated seawater was investigated by Wang et al. and their research revealed that the primary affinity for adsorption is electrostatic interaction and distribution diffusion mechanism (Wang et al., 2021b).

Polyamide (PA), also known as nylon, is a semi-crystalline polymer with a huge production volume. There are many types of PA plastics. Of these, the most commonly produced and used are polyamide 6 (PA6) and polyamide 66 (PA66), with annual production volumes of approximately 3.4 million and 4.4 million tons, respectively (Peng et al., 2020). Owing to their remarkable physical and mechanical properties, PA6 and PA66 are more prevalently used in fishing nets, cargo tie ropes, and aquaculture compared to other plastic products (Jiang et al., 2022). However, their wear and disposal give rise to copious amounts of PA6 and PA66 MPs in aquatic environments (Wang et al., 2018). In addition, their lower density (ρ = 1.00–1.15 g cm^{-3}) permits them to be effortlessly transported in water and perhaps serve as vessels for pollutants (Tang et al., 2021a). Therefore, the presence of PA6 and PA66 in aquatic environments may present a greater hazard. Although the monomer structures of PA6 and PA66 share similarities, the distinctness in their chemical properties stems from differences in synthetic procedures. However, the difference in the synthesis process will make the hydrogen bond strength of PA6 and PA66 different (Dasgupta et al., 1996). This may lead to differences in the adsorption of pollutants on PA6 and PA66. However, the research conducted on the adsorption behavior of pollutants on PA6 and PA66 is inadequate.

The use and production of dyes have grown in tandem with the progression of society, resulting in a surge of dye pollutants that discharge into aquatic environments through dilution (Haounati et al., 2021). These pollutants exhibit potent toxicity and can induce acute or chronic illnesses in organisms (Choudhary et al., 2020). Methyl orange (MO), an azo anionic dye, serves primarily as an acid-base indicator and for textile dyeing, while malachite green (MG), a triphenylmethane cationic dye, finds common use in dyeing silk and paper (Zhang et al., 2018; Mohammad et al., 2019). These dyes manifest strong inductive and carcinogenic properties, and their long-term exposure can instigate vomiting, tissue necrosis, and other maladies in organisms (Guo et al., 2011). Moreover, dye pollutants prove difficult to degrade and their prevalence renders inevitable contact with MPs. When MPs and dyes show affinity, contaminated MPs intensify environmental perils. Du et al. performed adsorption studies of the cationic dye crystal violet on naturally aged PE and PP, substantiating the strong affinity between crystal violet and MPs (Du et al., 2022). You et al. analyzed the adsorption-desorption behavior of methylene blue (MB) on both aged and unaged PE, thereby determining that PE could serve as a potential carrier for MB transportation (You et al., 2021). Nevertheless, studies that explore the interaction between dyes and MPs remain scant. In reality, wastewater that discharges into aquatic environments frequently contains more than one type of dye, and interactions between two or more dyes undeniably produce complex environmental behavior (Verma et al., 2021; Juang et al., 2010). Hence, the study of adsorption of binary or multiple dyes on MPs holds practical significance.

In this study, the anionic dye Methyl Orange (MO) and cationic dye Malachite Green (MG) were chosen as exemplary pollutants for the examination of their adsorption behavior on PA6 and PA66. The overarching objectives of this study were the following: (1) to study the adsorption behavior of MO and MG on PA6 and PA66, respectively; (2) to study the influence of environmental factors on the adsorption and desorption behavior of the two PAs after contamination; (3) to investigate the absorption behavior of PA6 and PA66 in the coexistence system of the two dyes; (4) to delve into the conceivable interaction mechanisms between the dyes and the two PAs. This study aims to foster a deeper comprehension of the possible environmental perils and provide a foundation for the composite pollution of multiple dyes on MPs.

2. Materials and methods

2.1. Materials and chemicals

Polyamide 6 and Polyamide 66 MPs (both with sizes ranging from 75 to 150 (m) were purchased from Hengfa Plasticization Co. Ltd

(Guangdong, China). Methyl orange (MO, ≥98%), malachite green (MG, ≥98%), and sodium taurocholate (NaT, ≥97%) were purchased from Aladdin Co. Ltd (Shanghai, China). The specific physical and chemical properties of the MPs and dyes are shown in Table S1. Fulvic acid (FA, ≥90%) was purchased from Domatte Technology Co. Ltd (Beijing, China). Methanol and acetonitrile of chromatographic grade were purchased from Sigma-Aldrich (St. Louis, MO, USA). High-purity water was obtained using a Milli-Q system (Bedford, MA, USA). Other reagents and chemicals (except MPs) used in the experiment were at least of analytical grade or higher. The MPs were washed three times with deionized water and ethanol to remove any possible organic compounds on their surface. They were then dried in a vacuum oven at 50 °C for 36 h and stored in glass bottles for future use. The dyes were dissolved in deionized water as stock solutions (500 mg L^{-1}).

2.2. Characterization

The surface morphology and size of PA6 and PA66 were observed using a scanning electron microscope (SEM, Sigma 500, Zeiss, Germany). The specific surface area of the two PAs was evaluated by nitrogen adsorption-desorption isotherm using the Brunauer-Emmett-Teller (BET) model at 77.35 K (ASAP 2460, Micromeritics Co., USA). The changes in the surface functional groups of the two PAs before and after adsorption were characterized using a Fourier-transform infrared spectrometer (FTIR, Nicolet iS5, Thermo Fisher, USA). Zeta potential was measured by NanoZS (Malvern, UK) for the 2 PA at different pH. X-ray diffraction (XRD, D8 Advance, Bruker, Germany) was used to determine the crystallinity of the two PAs. In addition, the static contact angles of the two PAs were measured by a contact angle goniometer (SL250, Kino, USA).

The concentration of the dye in the single system was determined by a UV–visible spectrophotometer (UV-2550, Shimadzu, Japan). The UV detection wavelengths for MO and MG were 464 nm and 615 nm, respectively. For the concentration of the dye in the binary system, ultra-high performance liquid chromatography (UPLC, Dionex, USA) was used for separation and analysis (Wang et al., 2022a). Specific chromatographic conditions are described in the Supplementary Material.

2.3. Batch adsorption experiments

Batch adsorption of dye (MO or MG) on PA6 and PA66 was made in fresh water in triplicates. Blank (without MPs or dyes) was used to correct possible errors. Dye of different concentrations was diluted by adding deionized water to the stock solution. The adsorption kinetics, adsorption thermodynamics, and environmental factors were investigated.

For the kinetics of adsorption, 50 mg of either PA6 or PA66 and 50 mL of 10 mg L^{-1} dye (either MO or MG) was added to a 50 mL amber EPA vial. The pH of the reaction solution was 6.0. The samples were placed in a light-proof oscillator with the rotation rate of 160 rpm and temperature of 25 °C, with sampling taking place at fixed time intervals (0, 1, 2, 4, 8, 12, 24, 36, 48, 72 h). The kinetic experiments have demonstrated that 48 h is sufficient for reaching adsorption equilibrium. Therefore, the equilibrium time for subsequent adsorption experiments was set at 48 h. In the adsorption isotherm experiment, the initial dye (MG or MO) concentration ranged from 5 to 40 mg L^{-1} at 25, 35, and 45 °C. The effects of salinity, pH, and FA on the adsorption of MG or MO on the two PAs were also studied.

To adjust pH within 2.0–10.0, 0.1 M NaOH or HCl was used. A certain amount of NaCl was added to the solution to simulate different salinities between freshwater and seawater (0–3.5%). The solutions with different concentrations of FA (0–30 mg L^{-1}) were prepared to study the effect of dissolved organic matter on adsorption.

In addition, adsorption experiments were conducted on the coexistence of the dyes (MO and MG) on PA6 and PA66 in a binary system. To achieve this, 50 mg of either PA6 or PA66 was added to amber EPA vials, followed by the addition of a coexisting solution of MO and MG at a concentration of 10 mg L^{-1} in 50 mL. The pH of the solution was adjusted to a targeted value (pH 2–10), and the samples were rotated at 160 rpm in a light-proof oscillator at a constant temperature of 25 °C for 48 h. After the adsorption experiments, 2 mL of the reaction solution was taken and centrifuged at 10,000 rpm for 10 min. Then, 1.5 mL of the supernatant was taken for measurements.

2.4. Desorption experiments

After the adsorption experiments, PA6 and PA66 were collected and dried at room temperature. Subsequently, the dye-adsorbed PAs were subjected to desorption experiments under the following conditions: (a) deionized water (pH = 6–7), (b) 0.1 M $CaCl_2$ and 15 mM sodium taurocholate, 38 °C, pH = 4, (c) 0.1 M $CaCl_2$ and 15 mM sodium taurocholate, 18 °C, pH = 7–8. These three conditions were chosen as they emulate more accurately the desorption environments of contaminated MPs in their natural habitats (freshwater, intestinal fluids of warm-blooded animals, and certain digestive fluids of marine organisms) (Razanajatovo et al., 2018; Tang et al., 2021b).

A portion of 0.10 g of dried PA6 or PA66 was transferred to the aforementioned solutions of 100 mL for desorption experiments. These were conducted at 25 °C and were shaken in darkness for 48 h. Each sample was replicated three times.

2.5. Data analysis

The adsorption equilibrium of dyes (MO or MG) on the two PAs was computed by the following equation:

$$q_t = \frac{V(C_0 - C_t)}{m} \quad (1)$$

where q_t (mg·g^{-1}) and C_t (mg·L^{-1}) are the amount of dye adsorbed and the solution concentration at time t, respectively; C_0 (mg·L^{-1}) is the initial dye concentration; V (L) is the volume of the reaction solution; and m (g) is the mass of PA involved in the adsorption reaction.

In this study, kinetic, isotherm and model fitting are described in Supplementary Material.

Data were analyzed using SPSS software (version 23.0, Statistical Package for the Social Sciences Inc., Chicago, USA) for ANOVA. The comparison of means was determined by Duncan's multiple range test ($p < 0.05$). Results are presented as mean ± SD.

3. Results and discussion

3.1. Characterization of PAs

Fig. 1a and b displays the SEM images of PA6 and PA66, the MPs employed in the adsorption experiments. These two PAs are quite alike in their dimensions and exhibit irregular shapes. Their relatively rough surfaces, as seen in Fig. 1a2 and Fig. 1b2, possess only a few pores. The BET results (Table S2) indicate that the specific surface areas of PA6 and PA66 are 0.287 and 0.296 m^2 g^{-1}, respectively, which is comparable to those reported in other studies for materials such as PVC (0.144 m^2 g^{-1}) (Jiang et al., 2020), PE (0.265 m^2 g^{-1}) and PS (0.621 m^2 g^{-1}) (Sun et al., 2022). Notably, the pore volumes of PA6 and PA66 are 7.28 and 3.02 mm^3 g^{-1}, respectively, which substantiates the SEM observations of two PAs having a sparse number of pores. Hence, it can be concluded that specific surface area and pore adsorption are not the primary factors contributing to the dye adsorption on PA6 and PA66.

Fig. S1 displays the FTIR spectra of both PAs before and after the adsorption of MO and MG. The spectra reveal that the characteristic peaks of the amide I (N–C═O stretching vibration) and amide II (C–N–H bending vibration) bonds of PA6 are at 1634 cm^{-1} and 1539 cm^{-1}, respectively (Guo and Wu, 2008). The peaks at 3294 cm^{-1}, 2934 cm^{-1},

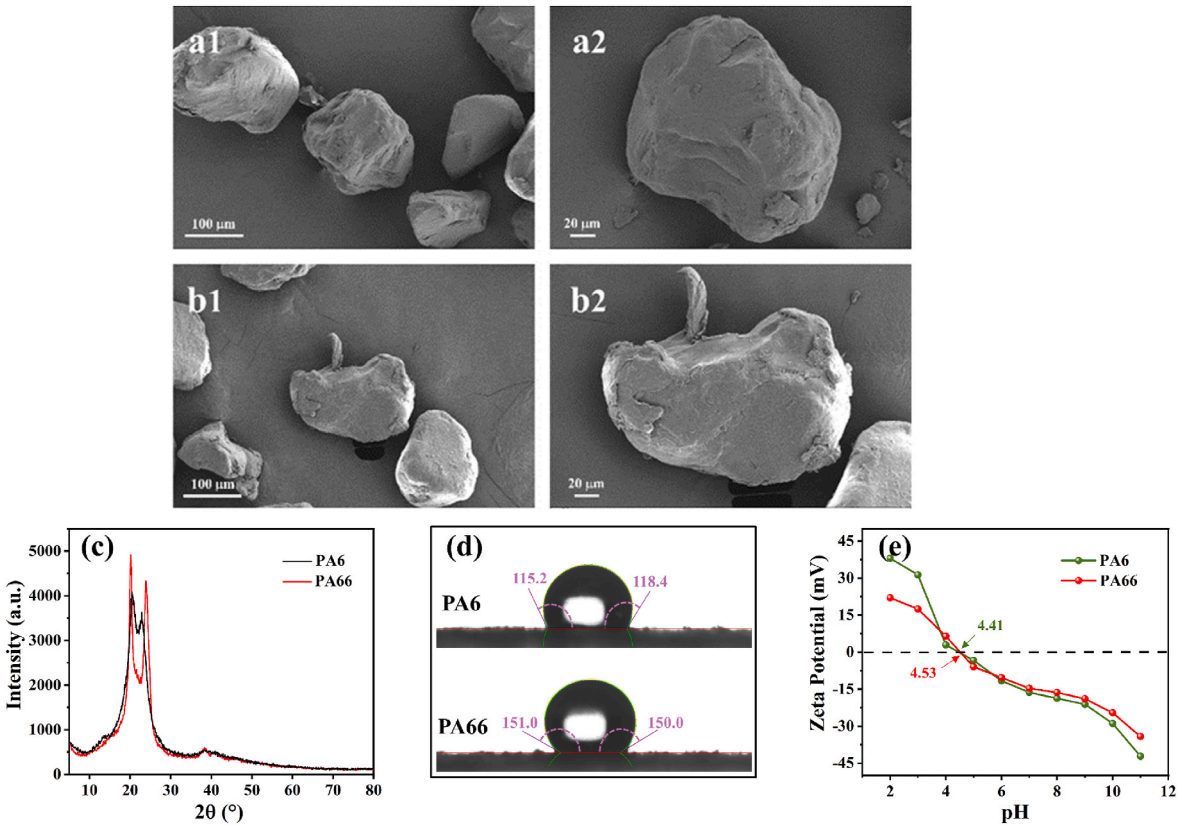

Fig. 1. SEM images of (a) PA6 and (b) PA66; (c) XRD, (d) contact angle and (e) zeta potentials (f) of PA6 and PA66.

and 2862 cm^{-1} are associated with N–H, C–H, and C–H stretching vibrations, respectively (Saleh and Ali, 2018). The FTIR spectrum of PA66 is nearly identical to that of PA6, given their highly similar molecular structure (Ma et al., 2016). No new peaks were detected in the FTIR spectra after the adsorption of MO and MG, indicating the absence of any new chemical bonds formed during the adsorption process.

XRD analysis was employed to determine the crystallinity of PA6 and PA66, as depicted in Fig. 1c. The results indicate that the diffraction peaks of PA66 are more pronounced and sharper than those of PA6, denoting a higher degree of crystallinity (Dasgupta et al., 1996). The crystallinity of PA66 (46.52%) was also computed using Jade 6.0 calculations, and it was found to be higher than that of PA6 (9.12%). Compared to high-crystallinity MPs, low-crystallinity MPs have more amorphous regions that are loose and flexible, making them more susceptible to dissolving and adsorbing pollutants (Zhao et al., 2020). Furthermore, contact angle measurements confirmed that both PA6 and PA66 are hydrophobic, with PA66 displaying a stronger hydrophobicity, as seen in Fig. 1d. The greater the hydrophobicity of the MPs, the more significant their hydrophobic effect, which has a positive influence on the adsorption of bisphenol contaminants by PVC, as reported by Wu et al. (2019).

To determine the electrostatic interaction between the PAs and the dye, zeta potential tests were performed on PA6 and PA66, as presented in Fig. 1e. Both PAs exhibited a continuous decline in zeta potential as the pH increased, with zero potential occurring near pH 4.5. Moreover, the absolute value of zeta potential for PA6 was higher than that of PA66 within the measured range, validating the former's greater sensitivity to pH changes in the system. The dissimilarities in the physical and chemical properties of PA6 and PA66 can be attributed to differences in their respective synthesis processes.

3.2. Sorption kinetics

In Fig. 2a–b, the adsorption kinetics of MO and MG on two PAs are presented. Generally, the adsorption of both MO and MG on both PAs increases with time until reaching equilibrium at 48 h. PA6 exhibits a higher adsorption capacity for both MO and MG compared to PA66. Fig. S2 shows the color comparison of the two PAs before and after the adsorption of MO and MG. The deepening of color further indicated that the adsorption of dye on PA6 is higher than that on PA66. To investigate the adsorption mechanism, the above kinetic data were fitted, and the results are shown in Table S3. The results indicate that the adsorption capacity of the pseudo-second-order (PSO) kinetic model ($R^2 > 0.981$) better fits the experimental data compared to the pseudo-first-order (PFO) kinetic model ($R^2 < 0.979$). Thus, the adsorption process is described as PSO, indicating that physical and chemical adsorption is in a control position (Yu et al., 2022). Furthermore, the Elovich model was used to further determine the potential adsorption mechanism based on the kinetic data. The Elovich model fits the data well, indicating that the surface adsorption energy may be non-uniformly distributed, and the adsorption process is a non-uniform diffusion process (Xue et al., 2021).

The mass transfer of dyes (MO and MG) from the bulk solution to the solid phase (PA6 and PA66) surface is related to physical adsorption, and the mass transfer process can be divided into three steps: external diffusion (surface adsorption), internal diffusion (pore diffusion), and adsorption onto active sites (Li et al., 2022). In most cases, the dominant factor affecting the adsorption rate is internal or external diffusion, or both simultaneously controlled (Wu et al., 2019). Sheng et al. studied the adsorption process of triclosan (TCS) on PE, PP, and PVC and confirmed that the adsorption of the three MPs on TCS is mainly through external diffusion and surface adsorption (Sheng et al., 2021). Yu et al. reported that the adsorption of tetracycline (TC) on PE was dominated by external and internal diffusion (Yu et al., 2020b). These reports demonstrate that the adsorption mechanisms between MPs and

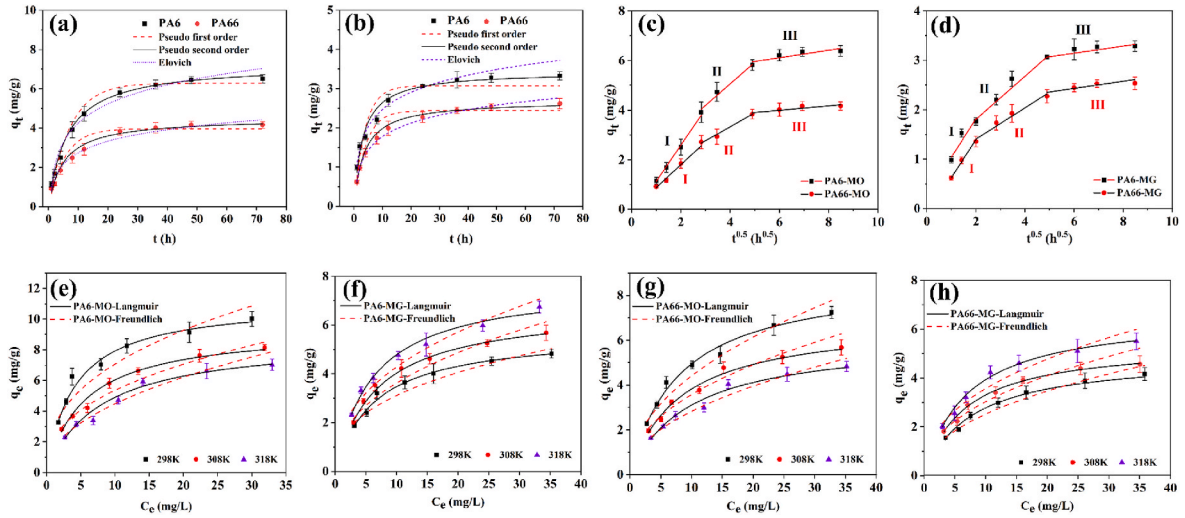

Fig. 2. Fitted kinetic curves by the model of PFO, PSO, Elovich equation (a and b) and intra-particle-diffusion (c and d), and fitted isotherms curves by the model of Langmuir and Freundlich (e–h).

pollutants are different, and their rate-limiting steps are also different. To further determine the controlling factors of the adsorption process of MO and MG on two PAs, the particle internal diffusion model was used to analyze the adsorption data, and segmented linear regression was used for fitting, as shown in Fig. 2c–d and Table S4. It is evident that the adsorption of MO and MG on both PAs follows three stages: external diffusion, internal diffusion, and quasi-equilibrium. The initial slope of the fitted data is greater than the subsequent slope, indicating that the external diffusion rate is higher than the internal diffusion and quasi-equilibrium during the adsorption process. The order of K_{ip} for PA6 and PA66 in the three stages is consistent with their adsorption capacity. The larger the value of C_i, the greater the boundary layer effect (Sulaymon and Abood, 2013; Wang et al., 2019). The order of intercepts is $C_1 < C_2 < C_3$, which means that the boundary layer effect is continuously increasing. Furthermore, the fact that C_i is not equal to zero confirms that internal diffusion is not the only rate-limiting step and that both external and internal diffusion play important roles throughout the entire adsorption process.

3.3. Adsorption isotherms and thermodynamics

In exploring the adsorption process of MO and MG on two PAs at different temperatures, we employed the Langmuir and Freundlich models (Fig. 2e–h and Table 1).

The Langmuir model posits that adsorption occurs as a single layer on a homogeneous surface, while the Freundlich model assumes adsorption occurs on a heterogeneous surface and is better suited for multi-layer adsorption (Fan et al., 2021). As depicted, the Freundlich model's linear fit was comparatively weak, implying that the adsorption process of MO and MG on the two PAs aligns more with single-layer adsorption on a homogeneous surface. The Langmuir model fits the adsorption data well, corroborating previous research findings (Li et al., 2018; Tang et al., 2020). Notably, R_L (Eq. (2)) signifies the adsorption characteristic value derived from the Langmuir model:

$$R_L = \frac{1}{1 + k_L C_0} \tag{2}$$

An R_L value less than one signifies favorable adsorption, whereas an R_L greater than one denotes unfavorable adsorption ($R_L = 1$, as linear) (Hall et al., 1966). From Tables 1 and it is evident that all the adsorption data R_L values fall between 0 and 1 (0.289–0.492), signifying that the adsorption of MO and MG on the two PAs is favorable. At room temperature, the maximum adsorption amounts of MG on PA6 and PA66 are 3.04 and 2.71 mg g^{-1}, respectively. The result is higher than Hexabromocyclododecane-PS and PVC, and comparable to that of nylon rope. In addition, the adsorption capacity of MO on PA6 and PA66 is 6.45 and 4.16 mg g^{-1}, which is higher than that of the (PE + polyethylene glycol) particle, as listed in Table S5.

Thermodynamic experiments are conducted to evaluate whether the dye adsorption reactions on two PAs occur spontaneously based on the van 't Hoff equation (Choudhary et al., 2020). The expressions are as follows:

$$\Delta G^{\circ} = -RTlnk_d \tag{3}$$

Table 1
Adsorption isotherm parameters of dye (MO and MG) onto PAs at different temperatures.

Dyes	MPs type	Temperature (K)	Langmuir model				Freundlich model		
			K_L (L·mg^{-1})	q_m (mg·g^{-1})	R^2	R_L	k_f (mg·g^{-1}·(mg·L^{-1})$^{1/n}$)	n	R^2
MO	PA6	298	0.2442	11.1588	0.988	0.289	2.8721	2.5571	0.932
		308	0.1788	9.4112	0.984	0.359	2.4280	2.5571	0.974
		318	0.1264	8.7688	0.974	0.442	1.5065	2.1143	0.950
	PA66	298	0.1265	8.8538	0.994	0.442	1.4658	2.1824	0.958
		308	0.1233	6.9186	0.978	0.448	1.2430	2.0917	0.948
		318	0.1034	6.1015	0.983	0.492	0.9250	2.0645	0.966
MG	PA6	298	0.1486	5.6856	0.993	0.402	1.2886	2.6124	0.965
		308	0.1569	6.7393	0.993	0.389	1.3556	2.3429	0.958
		318	0.1627	7.7211	0.993	0.381	1.6430	2.4039	0.957
	PA66	298	0.1296	4.9158	0.975	0.436	0.8757	2.1793	0.969
		308	0.1530	5.4619	0.992	0.395	1.1098	2.2943	0.971
		318	0.1581	6.6299	0.992	0.387	1.3549	2.3792	0.945

$$ln\ k_d = -\frac{\Delta H^\circ}{RT} + \frac{\Delta S^\circ}{R} \quad (4)$$

ΔG° (kJ·mol^{-1} K^{-1}), ΔH° (kJ·mol^{-1}), and ΔS° (J·mol^{-1}) are the Gibbs free energy, enthalpy, and entropy, respectively. R (8.314 J mol^{-1} K^{-1}) is the gas constant, and T (K) is the temperature, and k_d is the thermodynamic equilibrium constant, which is calculated from the dimensionless ratio of the equilibrium adsorption quantity (q_e) to the equilibrium concentration (C_e) (Xue et al., 2021).

The thermodynamic data for the adsorption of MO and MG on two PAs at three different temperatures, 298 K, 308 K, and 318 K, have been computed using the van 't Hoff equation, with the resulting changes in entropy (ΔS°), enthalpy (ΔH°), and Gibbs free energy (ΔG°) shown in Table S6. The negative values of ΔG° for both MO and MG on two PAs (−18.701 ~ −15.109 kJ mol^{-1}) suggest that the adsorption process is spontaneous and does not require external energy within the specified temperature range (Tang et al., 2020).

The magnitude of ΔH° may provide insights into the adsorption mechanism, with values less than 40 kJ mol^{-1} indicating physical adsorption and values greater than 40 kJ/mol indicating chemical adsorption (Chen et al., 2021). Thus, the adsorption of MO and MG on PA6 and PA66 is mainly affected by physical adsorption (ΔH° < 40 kJ mol^{-1}), which may suggest that hydrogen bonds, electrostatic attraction, and van der Waals forces are the dominant forces during the adsorption process. The negative values of ΔH° for MO (−19.637 and −17.916 kJ mol^{-1}) indicate that its adsorption process on PA6 and PA66 is exothermic. This phenomenon is consistent with the adsorption of most organic pollutants on MPs (Chen et al., 2021; Mohamed et al., 2020). ΔG° increases with elevated temperature, which indicates that MO adsorption is more favorable at a lower temperature. The increase in temperature leads to the breaking of hydrogen bonds, which further confirms the decrease in adsorption due to elevated temperature (Bao et al., 2021). On the other hand, the positive values of ΔH° for MG on PA6 and PA66 (14.233 and 16.918 kJ mol^{-1}) indicates that its adsorption on two PAs is endothermic. This phenomenon has been confirmed in related reports (Li et al., 2021b). The increase of temperature shifts the equilibrium constant towards a higher value, and the concentration of adsorbate on the surface of the adsorbent is higher.

The conclusions drawn from the differences in ΔG° and ΔH° for MO and MG on two PAs are consistent with the results of the adsorption isotherm experiments (Fig. 2e–h). Furthermore, the positive values of ΔS° (100.766 and 107.500 J mol^{-1}) indicate an increase in the randomness of the solid/liquid interface during the MG adsorption process with increasing temperature (Xue et al., 2021). Conversely, the ΔS° values of MO and the two PAs (−4.074 and −4.298 J mol^{-1}) are negative, suggesting a decrease in the concentration of MO at the solid/liquid interface and an increase in the concentration at the solid surface (Sheela et al., 2012).

3.4. Effects of salinity and fulvic acid concentration

To simulate the salinity levels found in natural aquatic environments, including rivers, lakes, and oceans (with salinity levels of approximately 3.5%), varying concentrations of NaCl were utilized to examine the adsorption behavior of MO and MG on the MPs. The findings of this study, as presented in Fig. 3a and c, and Table S7, revealed that the adsorption levels of MO and MG on the two PAs decreased notably as salinity levels increased.

In natural water, dissolved organic matter (DOM) is ubiquitous (Wang et al., 2022b). Fulvic acid (FA) is one of the key components of DOM, so the influence of FA on the adsorption of MO and MG should be discussed. Fig. 3b and d and Table S7 illustrate the effects of varying FA concentrations on the adsorption of MO and MG. The findings reveal that a low concentration of FA insignificantly affects the adsorption of MO and MG. However, when FA concentration increases (above 10 mg L^{-1}), the adsorption capacity of both MO and MG on the two types of

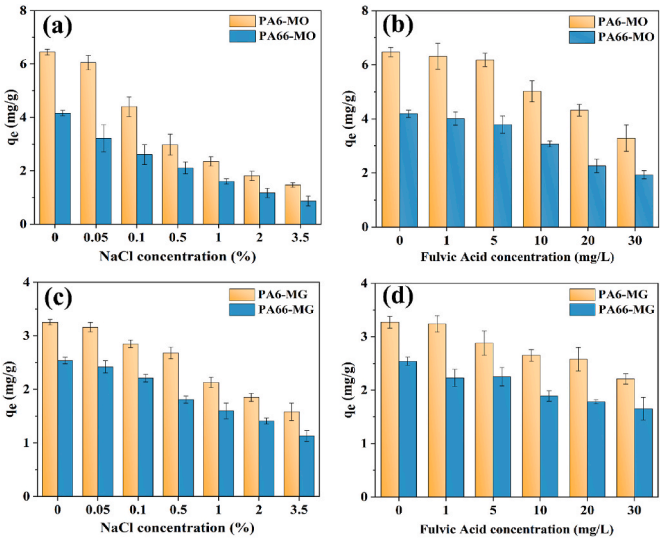

Fig. 3. Effects of salinity (a, c) and FA (b, d) upon the adsorption of dye by PA6 and PA66.

polyamides (PAs) significantly decreases. Upon adding 30 mg L^{-1} FA, the adsorption capacity of MO on PA6 and PA66 reduces to 50.9% and 46.1%, respectively, whereas that of MG on PA6 and PA66 reduces to 67.6% and 65.0%. Detailed information about the influence of salinity and fulvic acid concentration on the adsorption of MO and MG by the two PAs is presented in the Supplementary Material.

The above results demonstrate that PA6 and PA66 exhibit the same adsorption tendency for dyes even in solutions with different properties. To further elucidate this intriguing phenomenon, the underlying mechanism was subsequently revealed.

3.5. Effect of pH on adsorption

The pH of the environment plays a pivotal role in adsorption. Therefore, it is necessary to study the adsorption of dyes by PA at different pH in a single system. In the actual environment, the presence of multiple forms of dye contaminants renders the adsorption of a single dye on MPs insufficient to account for the authentic environmental state (Juang et al., 2010). Given this, we studied the impact of diverse pH values on the single and co-adsorption of PA6 and PA66, utilizing the prototypical ionic dyes MO and MG, as demonstrated in Fig. 4 and Table S8.

In single system, the adsorption of PA6 on MO increased, followed by a decrease, as the pH of the solution gradually increased. Conversely, the adsorption of MG by PA6 can be divided into two stages: slow and rapid increase with pH. The adsorption of dyes by PA66 and PA6 exhibited a consistent trend at the same pH, as shown in Table S8. Details of the effect of pH on adsorption in single systems are presented in the Supplementary Material.

Within the pH range of 2–10, the adsorption of MO and MG on both PAs in the binary system was lower than those in the single system, attributing to the existence of competitive adsorption. As depicted in Fig. 4a, MO held the dominant adsorption position at low pH (2–5), while MG took the leading position at high pH (9–10). When the pH was neutral (6–8), MO and MG exhibited strong competitive adsorption on PA6. At low pH, the adsorption capacity of MO was not notably reduced by the inclusion of MG; conversely, the adsorption capacity of MG in the binary system was significantly reduced. At low pH (excluding pH 4), electrostatic repulsion ensued between the dyes (MO and MG) and PA6. Thus, the apparent reduction of MG in the binary system may be attributed to the addition of MO, which reduces the hydrogen bonding between MG and PA6. This, in turn, corroborates the existence of

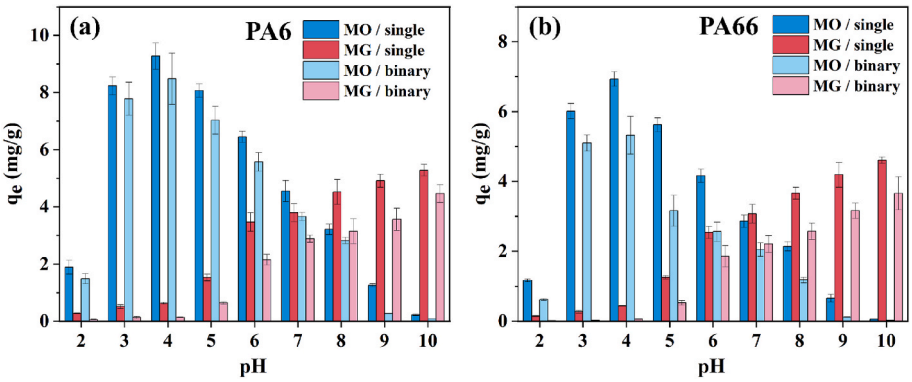

Fig. 4. Adsorption of MO and MG in the binary system by PA6 (a) and PA66 (b) at different pH.

hydrogen bonding between MG and PA6 and confirms that hydrogen bonding represents the principal cause for MO's domination of adsorption at low pH.

Compared to the single system, the adsorption of MG on both PAs in the binary system at high pH was slightly weakened. This phenomenon is ascribed to the presence of MO, which decreases the affinity between MG and PAs. At neutral pH, hydrogen bonds and electrostatic interactions between dyes (MO and MG) and PA6 engender strong competitive adsorption between MO and MG. As discerned from Fig. 4b, the adsorption capacity of PA66 for MO and MG was lower than that of PA6, while demonstrating the same pattern. Further examination is required to elucidate the adsorption discrepancy between PA6 and PA66 on dyes. The foregoing once again demonstrates that hydrogen bonding and electrostatic attraction are the primary mechanisms of adsorption for MO and MG.

3.6. Desorption efficiency

In Fig. 5, the desorption efficiency of the two PAs loaded with MO and MG exhibits a time-dependent increase under three distinct conditions. The variance in desorption is apparent under different circumstances. In Fig. 5a, the desorption efficiency of PA66 loaded with MO in simulated freshwater (deionized water) surpasses that of PA6 (5.12%) and reaches 14.75%. The desorption efficiency of PA6 and PA66 loaded with MO in simulated digestive tract fluid of marine organisms was the highest, reaching 36.98% and 45.69%, respectively, when compared to simulated intestinal fluid of freshwater and endothermic animals. In contrast, the desorption efficiency of PA6 and PA66 loaded with MG was the highest in the simulated digestive tract of endothermic animals, reaching 31.91% and 42.34%, respectively, in Fig. 5b. Furthermore, under the same conditions, the desorption efficiency of dye loaded PA66 is greater than that of PA6.

These findings indicate that PA66 exhibits a more substantial transport capacity for MO and MG than PA6, which might pose a greater environmental hazard. The desorption efficiency of adsorbed MO and MG varies significantly based on physiological conditions. MO is more likely to desorb from PA6 and PA66 into marine organisms, whereas MG is more likely to desorb from PA6 and PA66 into the intestinal fluids of endothermic organisms. Thus, PA6 and PA66 may enter biological tissues and other aquatic environments as carriers of MO and MG through the adsorption-desorption process, thereby increasing the risk of dye pollutants to aquatic organisms and human health. Additionally, the complexity of adsorption and desorption of diverse dye pollutants and PAs in the environment is validated.

3.7. Adsorption difference between PA6 and PA66

Our previous experiments have verified that the adsorption capacity of dyes onto PA6 is significantly higher than that of PA66. Interestingly, this difference is more pronounced in the adsorption of MO compared to MG. Our infrared data indicates that no new chemical bonds are formed during the adsorption process, suggesting that chemisorption is not the main reason for adsorption, as shown in Fig. S1. From a molecular structure perspective, both PA6 and PA66 have the same atomic ratios of C, H, O, and N. Their infrared spectra are almost identical (Ma et al., 2016). However, their production techniques differ significantly. PA6 is formed via head-to-end ring-opening polymerization of caprolactam, while PA66 is formed through the alternating formation of adipic acid and 1,6-hexanediamine (Lin et al., 2023). The synthesis process diagrams of PA6 and PA66 are shown in Fig. S4. These different monomer materials result in different polymer structures and physical properties, as demonstrated in Fig. 1 and Table S2. Moreover, the specific surface

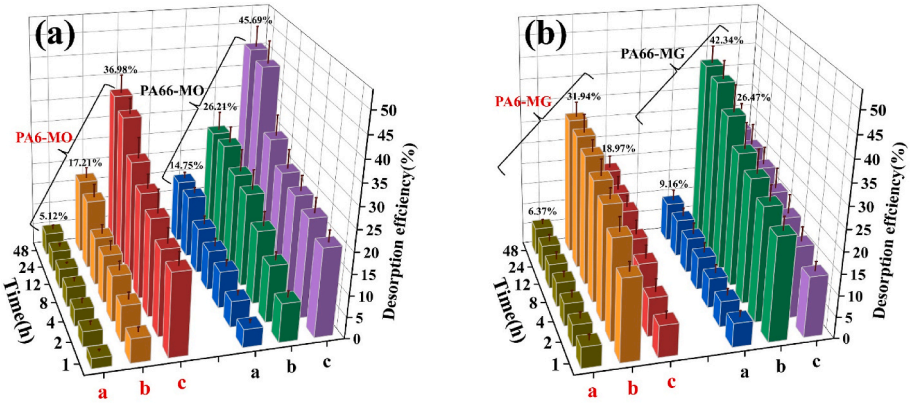

Fig. 5. Desorption efficiencies of dye within the time range of 0–48 h under various desorption conditions [(a) distilled water, 25 °C, pH = 7–8; (b) 0.1 M $CaCl_2$ and 15 mM sodium taurocholate, 38 °C, pH = 4; (c) 0.1 M $CaCl_2$ and 15 mM sodium taurocholate, 18 °C, pH = 7–8].

area of PA6 and PA66 used in our experiment is similar, indicating that specific surface area is not the main factor contributing to the difference in dye adsorption between these two PAs.

PA6 is significantly less crystalline than PA66, as shown in Fig. 1c and Table S2, indicating that there are more amorphous regions in PA6 that make it more prone to adsorb MO and MG (Song et al., 2021). Guo et al. (2012) have confirmed that the adsorption affinity of phenanthrene, naphthalene, and Lindane on the surface of PE decreases with increasing crystallinity, suggesting that lower crystallinity may also contribute to higher dye adsorption in PA6. Although the hydrophobicity of PA66 is higher than that of PA6, as demonstrated in Fig. 1d, the adsorption of dyes (MO and MG) onto PA66 is lower than that of PA6, confirming that hydrophobicity is not the main reason for the difference in dye adsorption between PA6 and PA66.

The adsorption experiments were carried out at pH 6.0, where the zeta potentials of PA6 and PA66 are similar, as shown in Fig. 1e. Thus, electrostatic interaction is not the main cause of adsorption differences. Instead, the unique structure and physical properties of polyamides (PA6 and PA66) are dominated by their hydrogen bonds (Shakiba et al., 2021). Therefore, the configuration and stability of hydrogen bonds in PA6 and PA66 significantly affect the adsorption process. Specifically, PA66 has only one stable hydrogen bond arrangement that is not affected by the *cis*-trans parallel arrangement, resulting in tight and stable hydrogen bonds in its amide bonds (Dasgupta et al., 1996; Lin et al., 2023). However, only half of the *cis*-trans parallel arrangement inside PA6 can form hydrogen bonds, and the configuration is relatively unstable (Wei et al., 2002; Li and Goddard, 2002). Additionally, the atomic arrangement regularity of PA6 is lower than that of PA66, as shown in Fig. S4. As a result, the unstable amide group in PA6 can more easily form hydrogen bonds with dyes compared to PA66. The tight the hydrogen bond arrangement, the higher the crystallinity, which is also the reason for the higher crystallinity of PA66 (Li and Goddard, 2002).

In the study conducted by Xiong et al. the adsorption behavior of ciprofloxacin and bisphenol with nano-PS was explored. It is believed that the weakening of the hydroxyl peak in the infrared spectra is a result of the formation of hydrogen bonds during adsorption (Xiong et al., 2020). As evident from Fig. S1a, the peak of the amide group at 1630 cm^{-1} and 1534 cm^{-1} of PA66 after adsorption of MO is noticeably weakened. On the other hand, the amide group peak of PA6 decreases to a greater extent. As a result, the adsorption of MO on PA6 is significantly higher than that of PA66, mainly due to stronger hydrogen bonding. Therefore, hydrogen bonding serves as the primary mechanism for MO adsorption on both PA6 and PA66. This observation may clarify the fact that although PA6 and PA66 differ only in terms of the adsorption amount, they exhibit the same adsorption trend. In contrast, the adsorption of MG by PA6 and PA66 is mainly attributed to electrostatic interaction. Hence, the strength of the hydrogen bond between MG and the two PAs has a limited influence on the adsorption amount.

5. Conclusion

In this study, we systematically investigated the adsorption behavior of two polyamides, PA6 and PA66, concerning two dye pollutants, MO and MG. Environmental experiments confirmed that the addition of NaCl and FA significantly hindered the adsorption process of MO and MG. We examined the effect of pH on the single and coexistence of MO and MG. In the single system, we observed that the adsorption capacity of MO increased initially and then decreased with increasing pH, whereas the adsorption capacity of MG increased continuously. In the binary system, our results indicated that at low pH (2–5), MO dominates adsorption on PA6 and PA66, whereas MG dominates at high pH (9–10), and strong competitive adsorption is observed at neutral pH (6–8). Furthermore, we conducted experiments and characterizations that confirmed that the adsorption of MO and MG on the two PAs was primarily influenced by hydrogen bonding and electrostatic attraction. The difference in adsorption between PA6 and PA66 on dyes is mainly attributed to the stability of the amide group and the difficulty of forming hydrogen bonds with pollutants. Desorption experiments revealed that the two PAs loaded with MO and MG exhibited desorption behavior in both simulated fresh water and simulated biological fluids. This indicates that PA can serve as a carrier of MO and MG, and can be transferred through adsorption-desorption behavior, posing a threat to the environment and biological health. In summary, our study of the adsorption behavior of PA6 and PA66 for two dyes contributes to our ability to accurately assess the environmental risks of the adsorption of single and co-existing dyes by different polyamides. In the future, more attention should be attached to the adsorption behavior between aged polyamide MPs and various dyes and their possible environmental risks.

Author contributions statement

Kangkang Wang: Experimental Investigation, Data analysis, Methodology, Writing - original draft. Yuli Kou: Investigation, Conceptualization, Formal analysis. Kefu Wang and Siqi Liang: Investigation, Validation, Formal analysis. Changyan Guo: Investigation, Resources. Yi Lu: Resources, Methodology, Funding acquisition, Supervision. Wei Wang and Jide Wang: Writing - review &editing, Funding acquisition. Project administration, Supervision.

Declaration of competing interest

The author declares that the publication of this paper does not involve a conflict of interest.

Data availability

No data was used for the research described in the article.

Acknowledgements

This research was financially supported by the National Natural Science Foundation of China (Grant No. 32061133005) and the Research Council of Norway (RCN, project 320456).

Appendix A. Supplementary data

Supplementary data to this article can be found online at https://doi.org/10.1016/j.chemosphere.2023.139806.

References

Bao, Z.Z., Chen, Z.F., Lu, S.Q., Wang, G., Qi, Z., Cai, Z., 2021. Effects of hydroxyl group content on adsorption and desorption of anthracene and anthrol by polyvinyl chloride microplastics. Sci. Total Environ. 790, 148077 https://doi.org/10.1016/j.scitotenv.2021.148077.

Barboza, L.G.A., Cunha, S.C., Monteiro, C., Fernandes, J.O., Guilhermino, L., 2020. Bisphenol a and its analogs in muscle and liver of fish from the north east atlantic ocean in relation to microplastic contamination. Exposure and risk to human consumers. J. Hazard Mater. 393, 122419 https://doi.org/10.1016/j.jhazmat.2020.122419.

Chen, Y., Li, J., Wang, F., Yang, H., Liu, L., 2021. Adsorption of tetracyclines onto polyethylene microplastics: a combined study of experiment and molecular dynamics simulation. Chemosphere 265, 129133. https://doi.org/10.1016/j.chemosphere.2020.129133.

Choudhary, M., Kumar, R., Neogi, S., 2020. Activated biochar derived from opuntia ficus-indica for the efficient adsorption of malachite green dye, Cu^{+2} and Ni^{+2} from water. J. Hazard Mater. 392 https://doi.org/10.1016/j.jhazmat.2020.122441.

Dasgupta, S., Hammond, W.B., Goddard, W.A., 1996. Crystal structures and properties of nylon polymers from theory. J. Am. Chem. Soc. 118, 12291–12301. https://doi.org/10.1021/ja944125d.

Du, H., Ma, H., Xing, B., 2022. Identification of naturally weathering microplastics and their interactions with ion dyes in aquatic environments. Mar. Pollut. Bull. 174, 113186 https://doi.org/10.1016/j.marpolbul.2021.113186.

Fan, X., Zou, Y., Geng, N., Liu, J., Hou, J., Li, D., Yang, C., Li, Y., 2021. Investigation on the adsorption and desorption behaviors of antibiotics by degradable mps with or without UV ageing process. J. Hazard Mater. 401, 123363 https://doi.org/10.1016/j.jhazmat.2020.123363.

Guo, Y., Wu, P., 2008. Ftir spectroscopic study of the acrylamide states in aot reversed micelles. J. Mol. Struct. 883–884, 31–37. https://doi.org/10.1016/j.molstruc.2007.11.009.

Guo, J., Du, Y., Lan, Y., Mao, J., 2011. Photodegradation mechanism and kinetics of methyl orange catalyzed by Fe(iii) and citric acid. J. Hazard Mater. 186, 2083–2088. https://doi.org/10.1016/j.jhazmat.2010.12.112.

Guo, X., Wang, X., Zhou, X., Kong, X., Tao, S., Xing, B., 2012. Sorption of four hydrophobic organic compounds by three chemically distinct polymers: role of chemical and physical composition. Environ. Sci. Technol. 46, 7252–7259. https://doi.org/10.1021/es301386z.

Hall, K.R., Eagleton, L.C., Acrivos, A., Vermeulen, T., 1966. Pore- and solid-diffusion kinetics in fixed-bed adsorption under constant-pattern conditions. Ind. Eng. Chem. Fund. 5, 212–223. https://doi.org/10.1021/i160018a011.

Haounati, R., Ouachtak, H., El Haouti, R., Akhouairi, S., Largo, F., Akbal, F., Benlhachemi, A., Jada, A., Addi, A.A., 2021. Elaboration and properties of a new sds/ctab@montmorillonite organoclay composite as a superb adsorbent for the removal of malachite green from aqueous solutions. Sep. Purif. Technol. 255 https://doi.org/10.1016/j.seppur.2020.117335.

Jiang, M., Hu, L., Lu, A., Liang, G., Lin, Z., Zhang, T., Xu, L., Li, B., Gong, W., 2020. Strong sorption of two fungicides onto biodegradable microplastics with emphasis on the negligible role of environmental factors. Environ. Pollut. 267, 115496 https://doi.org/10.1016/j.envpol.2020.115496.

Jiang, Z., Huang, L., Fan, Y., Zhou, S., Zou, X., 2022. Contrasting effects of microplastic aging upon the adsorption of sulfonamides and its mechanism. Chem. Eng. J. 430 https://doi.org/10.1016/j.cej.2021.132939.

Juang, R.-S., Lin, S.-H., Hsueh, P.-Y., 2010. Removal of binary azo dyes from water by uv-irradiated degradation in tio2 suspensions. J. Hazard Mater. 182, 820–826. https://doi.org/10.1016/j.jhazmat.2010.06.113.

Lee, H., Lee, H.J., Kwon, J.H., 2019. Estimating microplastic-bound intake of hydrophobic organic chemicals by fish using measured desorption rates to artificial gut fluid. Sci. Total Environ. 651, 162–170. https://doi.org/10.1016/j.scitotenv.2018.09.068.

Li, Y., Goddard, W.A., 2002. Nylon 6 crystal structures, folds, and lamellae from theory. Macromolecules (Washington, DC, U. S.) 35, 8440–8455. https://doi.org/10.1021/ma020815n.

Li, J., Zhang, K., Zhang, H., 2018. Adsorption of antibiotics on microplastics. Environ. Pollut. 237, 460–467. https://doi.org/10.1016/j.envpol.2018.02.050.

Li, H., Wang, F., Li, J., Deng, S., Zhang, S., 2021a. Adsorption of three pesticides on polyethylene microplastics in aqueous solutions: kinetics, isotherms, thermodynamics, and molecular dynamics simulation. Chemosphere 264, 128556. https://doi.org/10.1016/j.chemosphere.2020.128556.

Li, W., Xie, Z., Xue, S., Ye, H., Liu, M., Shi, W., Liu, Y., 2021b. Studies on the adsorption of dyes, methylene blue, safranin t, and malachite green onto polystyrene foam. Sep. Purif. Technol. 276 https://doi.org/10.1016/j.seppur.2021.119435.

Li, J., Huang, X., Hou, Z., Ding, T., 2022. Sorption of diclofenac by polystyrene microplastics: kinetics, isotherms and particle size effects. Chemosphere 290, 133311. https://doi.org/10.1016/j.chemosphere.2021.133311.

Lin, L., Ledesma-Amaro, R., Ji, X.J., Huang, H., 2023. Multienzymatic synthesis of nylon monomers from vegetable oils. Trends Biotechnol. 41, 150–153. https://doi.org/10.1016/j.tibtech.2022.08.006.

Liu, H., Jiao, Q., Pan, T., Liu, W., Li, S., Zhu, X., Zhang, T., 2023. Aging behavior of biodegradable polylactic acid microplastics accelerated by UV/H_2O_2 processes. Chemosphere 337, 139360.

Lončarski, M., Gvoić, V., Prica, M., Cveticanin, L., Agbaba, J., Tubić, A., 2021. Sorption behavior of polycyclic aromatic hydrocarbons on biodegradable polylactic acid and various nondegradable microplastics: model fitting and mechanism analysis. Sci. Total Environ. 785 https://doi.org/10.1016/j.scitotenv.2021.147289.

Ma, Y., Zhou, T., Su, G., Li, Y., Zhang, A., 2016. Understanding the crystallization behavior of polyamide 6/polyamide 66 alloys from the perspective of hydrogen bonds: projection moving-window 2d correlation ftir spectroscopy and the enthalpy. RSC Adv. 6, 87405–87415. https://doi.org/10.1039/c6ra09611e.

Missawi, O., Venditti, M., Cappello, T., Zitouni, N., Marco, G.D.E., Boughattas, I., Bousserrhine, N., Belbekhouche, S., Minucci, S., Maisano, M., Banni, M., 2022. Autophagic event and metabolomic disorders unveil cellular toxicity of environmental microplastics on marine polychaete hediste diversicolor. Environ. Pollut. 302, 119106 https://doi.org/10.1016/j.envpol.2022.119106.

Mo, Q., Yang, X., Wang, J., Xu, H., Li, W., Fan, Q., Gao, S., Yang, W., Gao, C., Liao, D., Li, Y., Zhang, Y., 2021. Adsorption mechanism of two pesticides on polyethylene and polypropylene microplastics: DFT calculations and particle size effects. Environ. Pollut. 291, 118120 https://doi.org/10.1016/j.envpol.2021.118120.

Mohamed, E.A., Selim, A.Q., Ahmed, S.A., Sellaoui, L., Bonilla-Petriciolet, A., Erto, A., Li, Z., Li, Y., Seliem, M.K., 2020. H_2O_2-activated anthracite impregnated with chitosan as a novel composite for Cr (VI) and methyl orange adsorption in single-compound and binary systems: modeling and mechanism interpretation. Chem. Eng. J. 380, 122445 https://doi.org/10.1016/j.cej.2019.122445.

Mohammad, A.T., Abdulhameed, A.S., Jawad, A.H., 2019. Box-behnken design to optimize the synthesis of new crosslinked chitosan-glyoxal/tio(2) nanocomposite: methyl orange adsorption and mechanism studies. Int. J. Biol. Macromol. 129, 98–109. https://doi.org/10.1016/j.ijbiomac.2019.02.025.

Na, J., Song, J., Achar, J.C., Jung, J., 2021. Synergistic effect of microplastic fragments and benzophenone-3 additives on lethal and sublethal daphnia magna toxicity. J. Hazard Mater. 402, 123845 https://doi.org/10.1016/j.jhazmat.2020.123845.

Peng, C., Tang, X., Gong, X., Dai, Y., Sun, H., Wang, L., 2020. Development and application of a mass spectrometry method for quantifying nylon microplastics in environment. Anal. Chem. 92, 13930–13935. https://doi.org/10.1021/acs.analchem.0c02801.

Razanajatovo, R.M., Ding, J., Zhang, S., Jiang, H., Zou, H., 2018. Sorption and desorption of selected pharmaceuticals by polyethylene microplastics. Mar. Pollut. Bull. 136, 516–523. https://doi.org/10.1016/j.marpolbul.2018.09.048.

Saleh, T.A., Ali, I., 2018. Synthesis of polyamide grafted carbon microspheres for removal of rhodamine b dye and heavy metals. J. Environ. Chem. Eng. 6, 5361–5368. https://doi.org/10.1016/j.jece.2018.08.033.

Shakiba, M., Rezvani Ghomi, E., Khosravi, F., Jouybar, S., Bigham, A., Zare, M., Abdouss, M., Moaref, R., Ramakrishna, S., 2021. Nylon—a material introduction and overview for biomedical applications. Polym. Adv. Technol. 32, 3368–3383. https://doi.org/10.1002/pat.5372.

Sheela, T., Nayaka, Y.A., Viswanatha, R., Basavanna, S., Venkatesha, T.G., 2012. Kinetics and thermodynamics studies on the adsorption of zn(ii), cd(ii) and hg(ii) from aqueous solution using zinc oxide nanoparticles. Powder Technol. 217, 163–170. https://doi.org/10.1016/j.powtec.2011.10.023.

Sheng, C., Zhang, S., Zhang, Y., 2021. The influence of different polymer types of microplastics on adsorption, accumulation, and toxicity of triclosan in zebrafish. J. Hazard Mater. 402, 123733 https://doi.org/10.1016/j.jhazmat.2020.123733.

Song, X., Wu, X., Song, X., Shi, C., Zhang, Z., 2021. Sorption and desorption of petroleum hydrocarbons on biodegradable and nondegradable microplastics. Chemosphere 273, 128553. https://doi.org/10.1016/j.chemosphere.2020.128553.

Sulaymon, A.H., Abood, W.M., 2013. Equilibrium and kinetic study of the adsorption of reactive blue, red, and yellow dyes onto activated carbon and barley husk. Desalination Water Treat. 52, 5485–5493. https://doi.org/10.1080/19443994.2013.814374.

Sun, M., Yang, Y., Huang, M., Fu, S., Hao, Y., Hu, S., Lai, D., Zhao, L., 2022. Adsorption behaviors and mechanisms of antibiotic norfloxacin on degradable and nondegradable microplastics. Sci. Total Environ. 807, 151042 https://doi.org/10.1016/j.scitotenv.2021.151042.

Tang, S., Lin, L., Wang, X., Feng, A., Yu, A., 2020. Pb(ii) uptake onto nylon microplastics: interaction mechanism and adsorption performance. J. Hazard Mater. 386, 121960 https://doi.org/10.1016/j.jhazmat.2019.121960.

Tang, S., Lin, L., Wang, X., Sun, X., Yu, A., 2021a. Adsorption of fulvic acid onto polyamide 6 microplastics: influencing factors, kinetics modeling, site energy distribution and interaction mechanisms. Chemosphere 272, 129638. https://doi.org/10.1016/j.chemosphere.2021.129638.

Tang, S., Lin, L., Wang, X., Yu, A., Sun, X., 2021b. Interfacial interactions between collected nylon microplastics and three divalent metal ions (cu(ii), ni(ii), zn(ii)) in aqueous solutions. J. Hazard Mater. 403, 123548 https://doi.org/10.1016/j.jhazmat.2020.123548.

Verma, S., Tirumala Rao, B., Singh, R., Kaul, R., 2021. Photocatalytic degradation kinetics of cationic and anionic dyes using au–zno nanorods: role of ph for selective and simultaneous degradation of binary dye mixtures. Ceram. Int. 47, 34751–34764. https://doi.org/10.1016/j.ceramint.2021.09.014.

Wang, Z., Su, B., Xu, X., Di, D., Huang, H., Mei, K., Dahlgren, R.A., Zhang, M., Shang, X., 2018. Preferential accumulation of small (<300 μm) microplastics in the sediments of a coastal plain river network in eastern China. Water Res. 144, 393–401. https://doi.org/10.1016/j.watres.2018.07.050.

Wang, J., Gao, M., Shen, T., Yu, M., Xiang, Y., Liu, J., 2019. Insights into the efficient adsorption of rhodamine B on tunable organo-vermiculites. J. Hazard Mater. 366, 501–511. https://doi.org/10.1016/j.jhazmat.2018.12.031, 2019.

Wang, Y., Wang, X., Li, Y., Li, J., Liu, Y., Xia, S., Zhao, J., 2021a. Effects of exposure of polyethylene microplastics to air, water and soil on their adsorption behaviors for copper and tetracycline. Chem. Eng. J. 404, 126412 https://doi.org/10.1016/j.cej.2020.126412.

Wang, X., Zhang, R., Li, Z., Yan, B., 2021b. Adsorption properties and influencing factors of cu(ii) on polystyrene and polyethylene terephthalate microplastics in seawater. Sci. Total Environ. 812, 152573 https://doi.org/10.1016/j.scitotenv.2021.152573.

Wang, K., Wang, M., Kou, Y., Guo, C., Ma, X., Tian, B., Qi, Y., Wang, W., Wang, J., 2022a. Determination of nitrofuran metabolites in meat products by uhplc-fluorescence with ultrasonic-assisted derivatization. J. Food Compos. Anal. 107, 104375 https://doi.org/10.1016/j.jfca.2021.104375.

Wang, Y., Liu, C., Wang, F., Sun, Q., 2022b. Behavior and mechanism of atrazine adsorption on pristine and aged microplastics in the aquatic environment: kinetic and thermodynamic studies. Chemosphere 292, 133425. https://doi.org/10.1016/j.chemosphere.2021.133425.

Wang, F., Zhang, Q., Cui, J., Bao, B., Deng, X., Liu, L., Guo, M.-y., 2023a. Polystyrene microplastics induce endoplasmic reticulum stress, apoptosis and inflammation by disrupting the gut microbiota in carp intestines. Environ. Pollut. 323, 121233 https://doi.org/10.1016/j.envpol.2023.121233.

Wang, K., Wang, K., Chen, Y., Liang, S., Guo, C., Wang, W., Wang, J., 2023b. Adsorption–desorption behavior of malachite green by potassium permanganate pre-oxidation polyvinyl chloride microplastics. Environ. Technol. Innov. 30, 103138 https://doi.org/10.1016/j.eti.2023.103138.

Wei, M., Davis, W., Urban, B., Song, Y., Porbeni, F.E., Wang, X., White, J.L., Balik, C.M., Rusa, C.C., Fox, J., Tonelli, A.E., 2002. Manipulation of nylon-6 crystal structures with its α-cyclodextrin inclusion complex. Macromolecules (Washington, DC, U. S.) 35, 8039–8044. https://doi.org/10.1021/ma020765m.

Wu, P., Cai, Z., Jin, H., Tang, Y., 2019. Adsorption mechanisms of five bisphenol analogues on pvc microplastics. Sci. Total Environ. 650, 671–678. https://doi.org/10.1016/j.scitotenv.2018.09.049.

Xiong, Y., Zhao, J., Li, L., Wang, Y., Dai, X., Yu, F., Ma, J., 2020. Interfacial interaction between micro/nanoplastics and typical ppcps and nanoplastics removal via electrosorption from an aqueous solution. Water Res. 184, 116100 https://doi.org/10.1016/j.watres.2020.116100.

Xue, X.D., Fang, C.R., Zhuang, H.F., 2021. Adsorption behaviors of the pristine and aged thermoplastic polyurethane microplastics in cu(ii)-otc coexisting system. J. Hazard Mater. 407, 124835 https://doi.org/10.1016/j.jhazmat.2020.124835.

You, H., Huang, B., Cao, C., Liu, X., Sun, X., Xiao, L., Qiu, J., Luo, Y., Qian, Q., Chen, Q., 2021. Adsorption-desorption behavior of methylene blue onto aged polyethylene microplastics in aqueous environments. Mar. Pollut. Bull. 167, 112287 https://doi.org/10.1016/j.marpolbul.2021.112287.

Yu, H., Yang, B., Waigi, M.G., Peng, F., Li, Z., Hu, X., 2020a. The effects of functional groups on the sorption of naphthalene on microplastics. Chemosphere 261, 127592. https://doi.org/10.1016/j.chemosphere.2020.127592.

Yu, F., Yang, C., Huang, G., Zhou, T., Zhao, Y., Ma, J., 2020b. Interfacial interaction between diverse microplastics and tetracycline by adsorption in an aqueous solution. Sci. Total Environ. 721, 137729 https://doi.org/10.1016/j.scitotenv.2020.137729.

Yu, Y., Li, H., Chen, J., Wang, F., Chen, X., Huang, B., He, Y., Cai, Z., 2022. Exploring the adsorption behavior of benzotriazoles and benzothiazoles on polyvinyl chloride microplastics in the water environment. Sci. Total Environ. 821, 153471 https://doi.org/10.1016/j.scitotenv.2022.153471.

Zhang, X., Lin, Q., Luo, S., Ruan, K., Peng, K., 2018. Preparation of novel oxidized mesoporous carbon with excellent adsorption performance for removal of malachite green and lead ion. Appl. Surf. Sci. 442, 322–331. https://doi.org/10.1016/j.apsusc.2018.02.148.

Zhao, L., Rong, L., Xu, J., Lian, J., Wang, L., Sun, H., 2020. Sorption of five organic ccompounds by polar and nonpolar microplastics. Chemosphere 257, 127206. https://doi.org/10.1016/j.chemosphere.2020.127206.